The Feasibility of Dynamic Height Determination from Moored Temperature Sensors

RAINER J. ZANTOPP AND KEVIN D. LEAMAN

Rosenstiel School of Marine and Atmospheric Science, University of Miami, Miami, FL 33149

(Manuscript received 16 May 1983, in final form 30 April 1984)

ABSTRACT

The existence of a tight T–S relationship in the southwestern North Atlantic is used to convert temperature measurements from moored sensors to dynamic heights. Seven hydrographic cruises with intensive CTD coverage during 1980–81 allow us to establish a close correlation between temperature and specific volume anomaly, which then is integrated vertically as a function only of temperature to derive dynamic heights. The systematic errors arising from the method are smaller than the natural variability of temperature from the mesoscale field.

1. Introduction

There has been considerable effort in the past to make use of the T–S relationship in most areas of the ocean in order to obtain dynamic heights and, subsequently, geostrophic shears from temperature measurements alone. Stommel (1947) first explored the possibility although he pointed out that C.-G. Rossby had originally suggested it. Several investigators have used existing T–S relationships in the Pacific (Emery, 1975; Emery and Wert, 1976), in the eastern North Atlantic (Siedler and Stramma, 1983) and in Gulf Stream rings (Flierl, 1978) to derive the dynamic height field based on temperature–depth measurements alone.

In this paper we will demonstrate the method and feasibility of dynamic height calculations from moored temperature sensors, a subject that has not been addressed in the past. The data set used is part of the Antilles Current experiment which took place in the southwestern part of the North Atlantic, east of the Bahamas between October 1980 and November 1981. Olson *et al.* (1984) describe the general hydrography of the area and the most recent findings about the Antilles Current which are to be used as a background for this paper.

2. The data set

The hydrographic observations around the Antilles Current moorings are well distributed in space and time: Four CTD cruises were carried out in the area, supplemented by three high-resolution surveys of the Ocean Tomography Experiment (OTE) (Ocean Tomography Group, 1982). Dates, numbers of stations and locations of all CTD stations used in this analysis are shown in Table 1 and Fig. 1, respectively.

All hydrographic measurements were taken with Neil Brown CTD instruments, with bottle data at appropriate depths for calibration purposes. Overall the cruise-specific calibrations were good (Table 1), and cruise-to-cruise differences are negligibly small. The OTE data were supplied to us in calibrated form as described in Behringer *et al.* (1982). All final CTD profiles are interpolated to 2 db intervals, all hydrographic variables are based on the UNESCO (1981) convention.

Four deep-water moorings, M125–M128, were deployed in the Antilles Current area between 10 November 1980 and 5 November 1981, two environmental moorings, W705 and W706, were placed in the center and at the southern border of the OTE array between 3 March and 9 August 1981. Locations are given in Fig. 1 and Table 2, mooring configurations and instrumentation in Table 3. All instruments were calibrated before deployment and checked after recovery. Only minor problems occurred in most of them and were subsequently corrected. However, the temperature sensor at 650 m at M125 stopped working on 3 June 1981, and the 3050 m instruments at M127 and M128 could not be retrieved.

All time series were low-pass filtered with a 40 h cutoff to eliminate tidal and inertial fluctuations.

3. Dynamic heights from temperatures

The western North Atlantic is known as a region with a rather tight relationship between temperature and salinity (e.g. Stommel, 1947; Emery, 1975). However, we will evaluate the relationship between temperature (T) and specific volume anomaly (δ_{STp}) instead. This does not add any particular insight into water mass analysis but is convenient for the calculation of dynamic heights. It is also (see Fig. 2) the most linear of all hydrographic relations to be considered here.

TABLE 1. Antilles Current Experiment: CTD surveys and standard errors on CTD calibration.

Data subset	Ship	Date	Number of stations	p (db)	T (°C)	S (ppt)
Fall 1980	*Researcher*	10/25–11/9/80	45	5	0.016	0.006
	Iselin	11/9–11/22/80	33	2	0.012	0.004
OTE 1	*Researcher*	3/7–3/24/81	65			
OTE 2	*Researcher*	4/30–5/19/81	75			
Summer 1981	*Iselin*	6/19–7/1/81	25	6	0.010	0.005
OTE 3	*Researcher*	7/8–7/26/81	79			
Fall 1981	*Iselin*	10/24–11/6/81	28	6	0.011	0.005

The possibility of a seasonal bias due to the unequally large CTD data sets over the course of the experiment is reduced to a large extent by combining each CTD subset—as defined in Table 1—into one realization of average salinity and pressure on isothermal surfaces with a 0.1°C increment (Fig. 2a, b). These mean profiles were then used to calculate specific volume anomaly (Fig. 2c) as a function of temperature. The evaluation of a seasonally changing T–S relation based on this data set did not yield significant differences. We will therefore look at the seasonally constant relationship only.

There are two major requirements for the determination of geostrophic shears from moored temperature measurements: a) knowledge of the actual instrument depths at all times and b) adjustment of the individually measured temperature $T(p)$ to a corresponding temperature T^* on constant pressure surfaces.

Moored pressure sensors were located at the 400 m level only for M125–M128. Under the assumption of a taut-wire, fixed-pendulum configuration we calculated the individual instrument depths from the pressure record, the wire lengths between instruments and the water depth at the mooring location. More sophisticated estimates did not produce significantly better results.

To correct the individually measured temperatures (T) to a temperature T^* at p^* = constant, we integrate the vertical temperature gradient dT/dz as a function of T over the depth range between the actual instrument depth z and the constant pressure

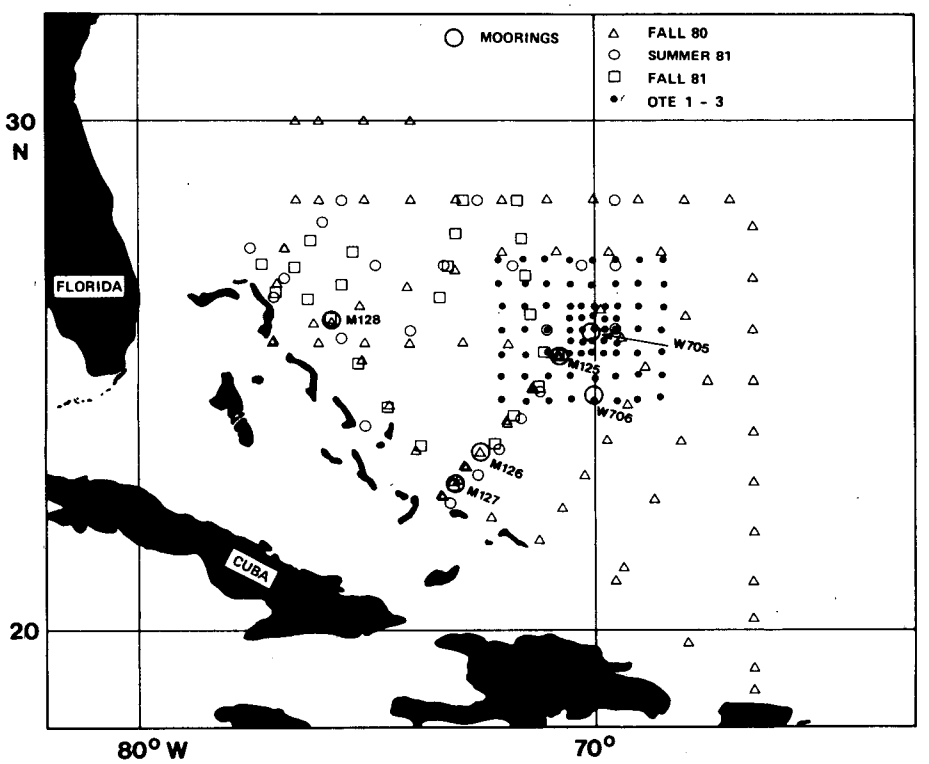

FIG. 1. Distribution of all CTD stations taken in the Antilles Current area between October 1980 and November 1981. Mooring locations are indicated by large open circles.

TABLE 2. Mooring locations and water depths.

Mooring	Latitude (N)	Longitude (W)	Water depth (m)
M125	25°29.1′	70°44.4′	5524
M126	23°38.2′	72°27.8′	5325
M127	22°59.0′	73°00.8′	4843
M128	26°12.1′	75°42.8′	4707
W705	25°57.3′	70°02.6′	5488
W706	24°46.1′	69°59.6′	5565

p^*, using the hydrostatic assumption to convert pressure to depth. Thus,

$$T^* = T + \int_z^{z^*} \frac{dT}{dz}(T)dz. \quad (1)$$

The use of the vertical temperature gradient as a function of temperature rather than depth is preferable, particularly around the 18°C water (Fig. 3) where the sharp minimum of dT/dz clearly identifies the isostad.

For each mooring and each depth level the dynamic height anomaly (ΔD) is then calculated from these adjusted temperatures T^* and the specific volume anomaly,

$$\Delta D = \int_{1050}^{z^*} \delta_{STp}(T^*)dp \quad (2)$$

with a reference level of 1050 m.

4. Comparison with CTD data

An important question to be answered here is how well the temperature-derived dynamic heights compare with the CTD data. In an attempt to obtain as many points of comparison as possible, we looked at all CTD stations within an 85 km radius of the moorings. Fig. 4a shows the correlation between temperature-derived and CTD-derived dynamic heights within 12 hours of each other. A slight overestimate in the mooring data is obvious, with a large noise level at all depths. However, as the dynamic-height differences (mooring minus CTD) in Fig. 4b indicate more clearly, most of the noise is due to the spatial variability of the dynamic-height field in the vicinity of the moorings (see Fig. 6). We then compare CTD stations within 30 km of the moorings (Fig. 5a–b) and find a slight improvement of the correlation, despite the fewer degrees of freedom for the fit. Regression coefficients and errors for both radii are listed in Table 4.

5. Time series of geostrophic velocity

The temperature-derived time series of dynamic height at several mooring locations enable us to estimate geostrophic velocities and tie those into the traditional picture of CTD surveys. Moorings M125, W705 and W706 are located within the Ocean Tomography Experiment box with its excellent CTD coverage (Ocean Tomography Group, 1982). The horizontal separation of these three moorings is also small enough so that we can hope to resolve adequately the scale of motion that was seen during OTE 1–3. We therefore do a plane fit of dynamic heights through the mooring positions at each depth level and scale the derivatives in x and y in order to obtain geostrophic velocities with a reference level of 1050 m.

$$u' = -\frac{10}{g}\frac{d(\Delta D)}{dy}, \quad (3)$$

TABLE 3. Mooring configurations.

M125–M128			W705			W706		
Instrument			Instrument			Instrument		
Depth (m)	Type	Variable sampled	Depth (m)	Type	Variable sampled	Depth (m)	Type	Variable sampled
200	VACM	*uvT*	137	VACM	*uvT*	251	VACM	*uvT*
300	TDR	*T*						
400	ACM	*uvTp*	368	TDR	*p*	435	TDR	*Tp*
650	TDR	*T*	617	TDR	*Tp*	678	TDR	*Tp*
700	NWCM	*uv*						
850	TDR	*T*	835	VACM	*uvT*	949	VACM	*uvT*
1050	VACM	*uvT*						
1550	VACM	*uvT*	1846	TDR	*Tp*	1926	TDR	*Tp*
3050	VACM	*uvT*	2838	TDR	*Tp*	2897	TDR	*Tp*

VACM Vector Averaging Current Meter
TDR Temperature–Depth Recorder
ACM Aanderaa Current Meter
NWCM Niskin Wing Current Meter

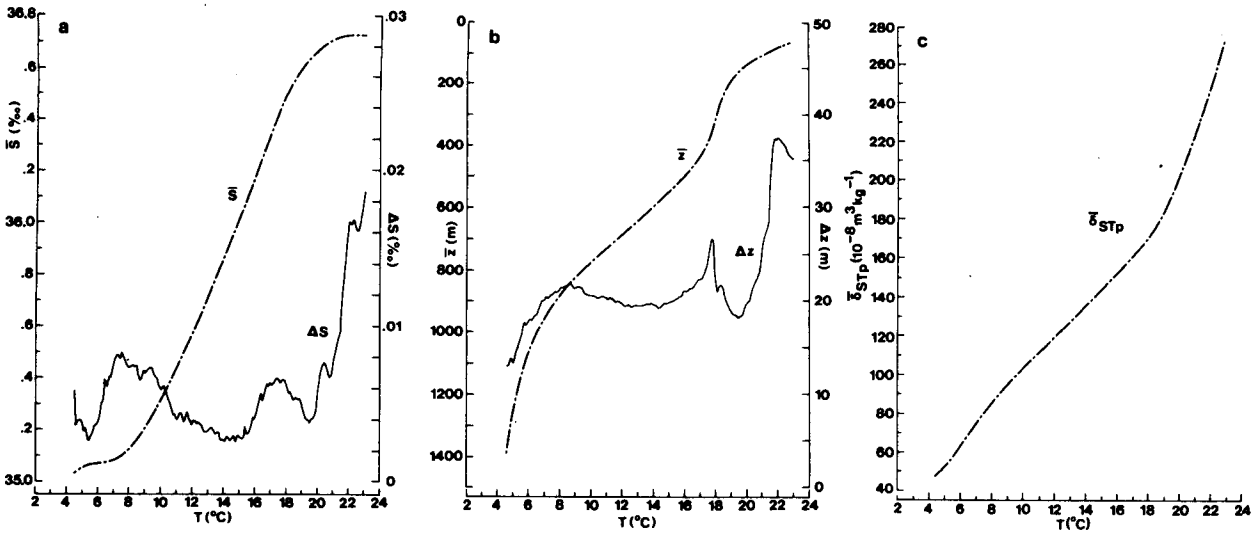

FIG. 2. Mean profiles and standard deviations of (a) salinity, (b) depth and (c) specific volume anomaly on temperature surfaces.

$$v' = \frac{10}{g}\frac{d(\Delta D)}{dx}. \tag{4}$$

In Fig. 6 we show maps of dynamic height 200–1050 m for OTE 1–3 (origin at 25°N, 75°W) and superimpose the positions of the three moorings and the geostrophic velocity vector 200–1050 m averaged over the length of the CTD survey. We also present the time series of geostrophic velocity 200–1050 m as calculated from the plane fit of temperature-derived dynamic heights. The periods of CTD surveys are indicated.

We find a generally good agreement between the flow pattern deduced from the CTD surveys and the geostrophic flow within the mooring triangle. During OTE1 the moorings are south of the intense cyclonic eddy that dominates the flow field until mid-April.

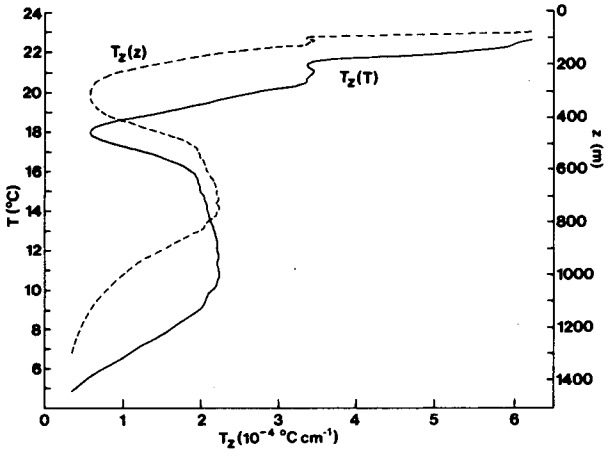

FIG. 3. Mean vertical temperature gradient as a function of temperature and depth, respectively.

OTE2 shows that a second eddy, of less intensity, has moved in from the east, and again we find south-easterly flow during this time period.

With the beginning of June this second eddy crosses the mooring triangle on its westward path, during which we find mainly northerly components in the geostrophic velocities, and during OTE3 we are in the transition phase between this last cold eddy and the approaching high-pressure system visible in the NE corner of the survey area. Geostrophic currents turn to the NE by the end of July with magnitudes of 20 cm s^{-1}.

The time series of geostrophic currents in conjunction with the OTE hydrographic surveys confirm the westward drift of the mesoscale eddy field that had been previously described by the Ocean Tomography Group (1982). We find qualitatively good agreement between both data sets. The uncertainty for the geostrophic current, based on a mean error of 0.01 dyn-m on each mooring, results in a 4 cm s^{-1} speed error.

6. Estimation of errors

To estimate the error in dynamic height anomaly ΔD caused by errors in specific volume anomaly (δ_{STp}), we will assume that at each of N pressure levels, we have

$$\hat{\delta}_j = \delta_j + \epsilon'_j, \quad j = 1, 2, \ldots, N, \tag{5}$$

where $\hat{\delta}_j$ is our estimate and ϵ'_j is the error. We can estimate ϵ'_j by

$$\epsilon'_j = \left.\frac{\partial\delta}{\partial S}\right|_j \Delta S_j + \left(\left.\frac{\partial\delta}{\partial S}\right|_j \left.\frac{d\bar{S}}{dT}\right|_j + \left.\frac{\partial\delta}{\partial T}\right|_j\right)\epsilon_{Tj} + \left.\frac{\partial\delta}{\partial p}\right|_j \epsilon_{pj}$$

$$= A_j\Delta S_j + B_j\epsilon_{Tj} + C_j\epsilon_{pj}. \tag{6}$$

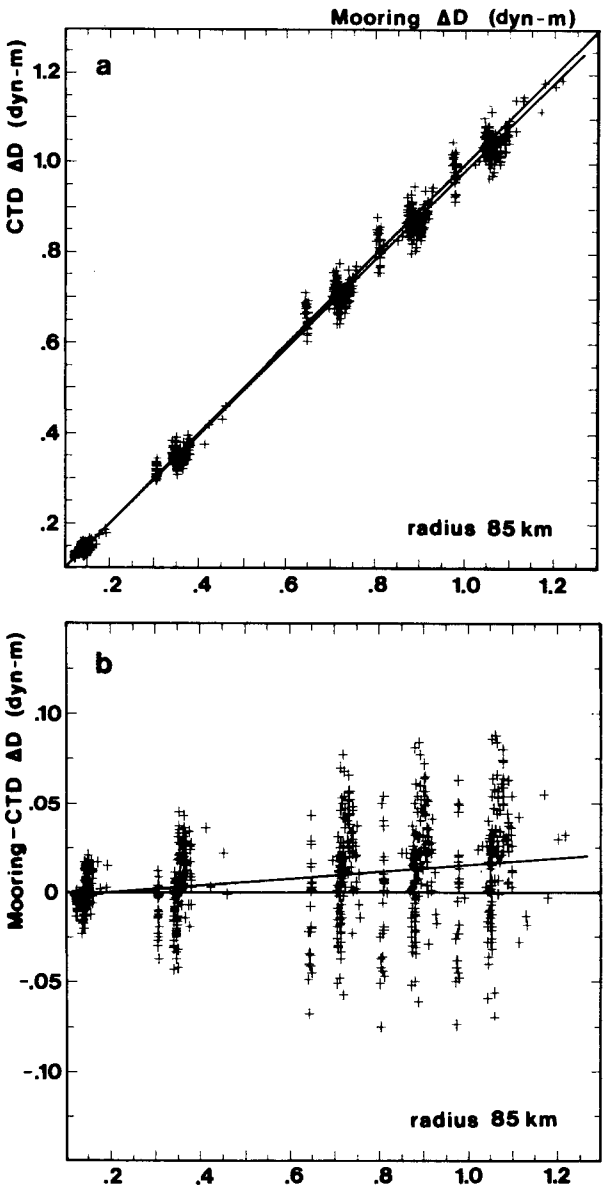

FIG. 4. (a) Scatter plot of dynamic heights from moorings vs CTD stations within a radius of 85 km. (b) Scatter plot of dynamic-height difference vs mooring dynamic heights within a radius of 85 km.

The first term accounts for the deviation ΔS_j of the actual T–S curve at a given depth from the mean curve $\bar{S}(T)$. The second term adds the direct error in δ caused by an error ϵ_{Tj} in temperature at a given sensor plus the error in salinity caused by using temperature to compute salinity through a mean T–S curve, where $d\bar{S}/dT|_j$ is the slope of that curve. The last term accounts for errors ϵ_{pj} in measuring pressure.

Some assumptions must be made about the nature of the S, T and p errors before reasonable estimates for the error in ΔD can be obtained. For the present study we have made the following assumptions:

1) The errors ϵ_{Tj} between different temperature sensors on a mooring are uncorrelated.

2) The natural variations ΔS_j in the T–S curve are uncorrelated with either instrumental temperature or pressure errors.

3) The variations ΔS_j are however perfectly correlated over the depth range of the mooring sensors. This argues in effect that the actual T–S curve, over a large depth range, tends to shift relative to the mean curve. Actual comparisons of individual T–S curves in the area of study with the mean curve indicate that this is a reasonable assumption.

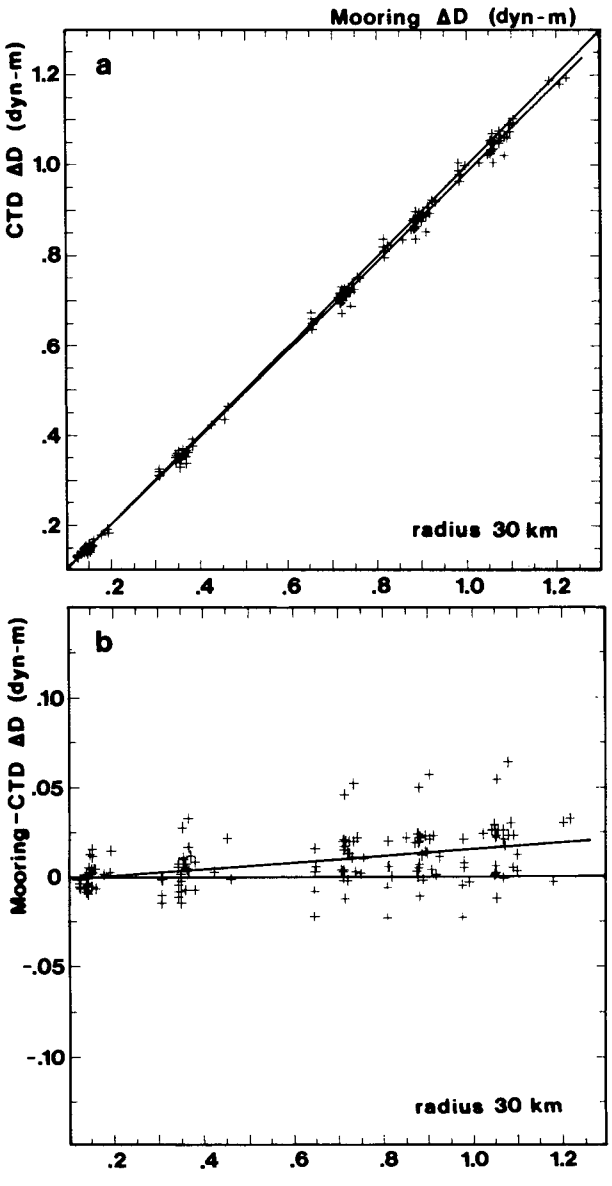

FIG. 5. (a) As in Fig. 4a but for radius of 30 km. (b) As in Fig. 4b but for radius of 30 km.

TABLE 4. Correlations and errors for dynamic height comparisons.

	Radius (km)	
	85	30
Number of CTD stations	154	31
Regression coefficient	0.9972	0.9992
rms error (dyn m)	0.0260	0.0151
Mean error (dyn m)	0.0080	0.0092

4) Pressure errors are also assumed to be essentially independent of depth and perfectly correlated over the depth range of the sensors. This assumption is a consequence of the method used to correct for mooring tilt.

We also assume that temperature and pressure errors are unbiased (i.e., that good calibrations were made).

To illustrate the effect of errors in δ on a numerical integration to obtain dynamic height anomaly, we use as an example a simple trapezoidal integration formula, where the error $\epsilon(\Delta D)$ is given by

$$\epsilon(\Delta D) = \frac{1}{2}\sum_{j-1}^{N-1}(\epsilon_j' + \epsilon_{j+1}')\alpha_j, \tag{7}$$

where $\alpha_j = p_{j+1} - p_j$ is the distance in pressure between two temperature sensors.

As an example we have used the parameters shown in Table 5 to estimate the variance of $\epsilon(\Delta D)$ for mooring 126. Although the parameters A_j, B_j and C_j in Eq. (6) strictly depend on depth, a reasonably accurate estimate of the variance of $\epsilon(\Delta D)$ can be obtained by using depth-averaged values from Table 5 (an overbar denotes a depth average): $\bar{A} = \overline{\partial\delta/\partial S} = -72.6 \times 10^{-5}$; $\overline{\partial\delta/\partial T} = 20.52 \times 10^{-5}$; $\bar{B} = \overline{(\partial\delta/\partial S)} \times (d\bar{S}/dT) + \overline{\partial\delta/\partial T} = 1.07 \times 10^{-4}$; $\bar{C} = \partial\delta/\partial p = 2.71 \times 10^{-7}$. Also the average slope of the mean T–S curve (Fig. 2) over the range of temperatures encountered is 0.135‰ (°C)$^{-1}$.

Finally, we need estimates for the variances associated with ϵ_T, ϵ_p and ϵ_S. Based on sensor accuracies the rms values for ϵ_T and ϵ_p are assumed to be 0.1°C and 10 db. Based on Fig. 2 a reasonable estimate for the rms value of ΔS errors (away from the surface) is 0.01‰.

With the above assumptions the expression for the variance of $\epsilon(\Delta D)$ is

$$\langle\epsilon^2(\Delta D)\rangle = (\bar{A}^2\langle\Delta S^2\rangle + \bar{C}^2\langle\epsilon_p^2\rangle)\sum_{i=1}^{N-1}\sum_{j=1}^{N-1}\alpha_i\alpha_j + \frac{\bar{B}^2}{2}\langle\epsilon_T^2\rangle\Big(\sum_{j=1}^{N-1}\alpha_j^2 + \sum_{j=2}^{N-1}\alpha_j\alpha_{j-1}\Big). \tag{8}$$

Substituting the values given above in Eq. 8 gives a variance for $\epsilon(\Delta D)$ of 1.44×10^{-8} (dyn m)^2, or an rms error in ΔD of 0.012 dyn m. (If the depth-dependence of A_j, B_j and C_j is taken into account this value is actually decreased slightly. This is primarily because the values of B_j and C_j are largest nearer the surface, where the integration increments (α_j) are smaller).

An examination of the contributions of the T, S and p errors to the variance of ΔD shows that approximately 70% of the variance comes from the ΔS term. This clearly demonstrates that any useful application of this method (including at least some attempt to estimate accuracy in determining ΔD) requires first that the T–S curve be tight and second that the statistical background of fluctuations in the T–S curve be known with some certainty. In the present experiment sufficient CTD profiles were made in an area with a relatively tight T–S relation so that this was the case. Misleading results could easily be obtained if one attempted to apply this method in a region with inadequate knowledge of the T–S structure.

7. Conclusions

In the southwestern North Atlantic, the tight T–S relationship makes it possible to convert temperature measurements to dynamic heights from moored sensors with a reasonably high accuracy. A comparison of these measurements to CTD stations within a 30 km radius of the moorings shows that the rms difference between the two methods for determining dynamic height is about 0.015 dyn m; some of this difference is certainly attributable to mesoscale variability in the temperature field itself.

A quantitative description of error sources has been given. In the case of the measurements described here, a primary source of error was the relatively sparse set of available pressure measurements. There is no doubt that additional pressure measurements on each mooring would result in an even higher level of accuracy in the computed dynamic heights. However, the error estimates quoted here will in any case allow one to make an *a priori* determination of the

TABLE 5. Gradients of specific volume anomaly for mooring 126.

Pressure (db)	Temperature (°C)	$\partial\delta/\partial T$ ($\times 10^{-5}$)	$\partial\delta/\partial p$ ($\times 10^{-7}$)	$\partial\delta/\partial S$ ($\times 10^{-5}$)
206	18.9	24.5	3.5	−72.3
306	18.0	23.9	3.35	−72.35
406	17.2	23.4	3.2	−72.3
656	12.8	20.0	2.7	−72.6
856	8.8	16.7	2.0	−73.0
1056	6.1	14.6	1.5	−73.25

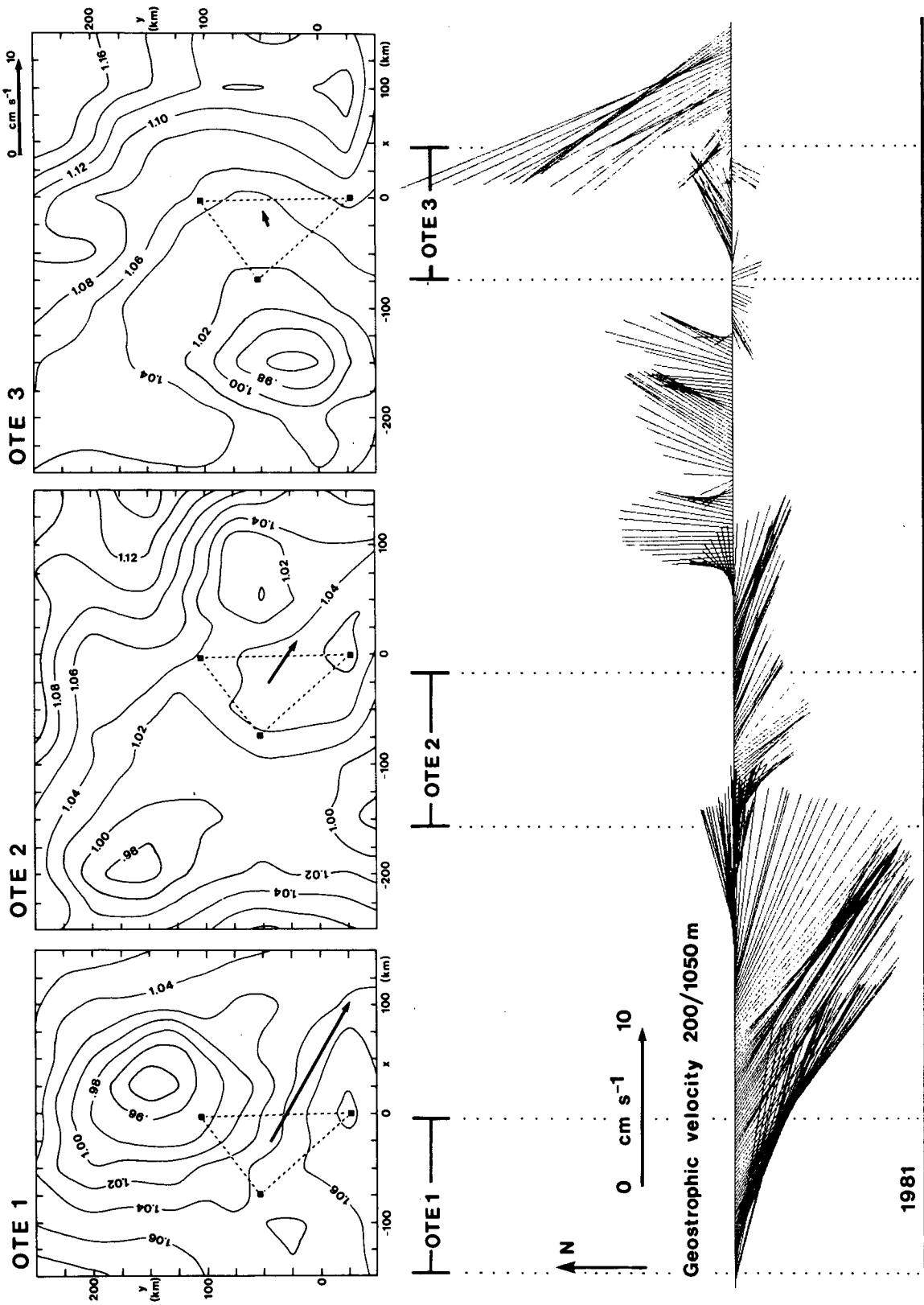

FIG. 6. Maps of dynamic height 200/1050 m for OTE 1–3, with mooring locations M125, W705 and W706. Geostrophic velocity vectors, derived from time series of dynamic height at moored temperature sensors are shown as stick plots. The vectors averaged over the time of the CTD surveys are shown on the dynamic-height maps.

feasibility of the method, given information on the T–S relation in the area under consideration, and also the configuration and accuracy of instrumentation to be used on moorings.

Acknowledgments. This paper was made possible as part of the Antilles Current experiment in which F. Schott and D. Olson were instrumental during all phases. We wish to thank them for their support. We also acknowledge the efforts of the Ocean Technology Group at the University of Miami under Phil Bedard and the help of Paula Diaz, Geoffrey Samuels and Peter Vertes with data processing.

The data set that our group has taken over the past several years in the Antilles Current region has greatly benefitted from generous support through the Ocean Tomography Experiment. David Behringer of NOAA/AOML provided 219 high-quality CTD profiles, and Robert Heinmiller and Carl Wunsch of MIT released the temperature and current measurements from the environmental moorings. They also helped to resolve a few data inconsistencies. We gladly acknowledge the permission of NOAA/AOML to participate in the RV *Researcher* cruise in October–November 1980, which significantly contributed to our objectives. This work was supported by the Office of Naval Research under Contract N00014-80-C-0042.

REFERENCES

Behringer, D., R. Heinmiller, R. Knox and G. Thomas, 1982: Environmental observations during the 1981 Ocean Tomography Experiment. NOAA Tech. Rep., 26 pp.

Emery, W. J., 1975: Dynamic height from temperature profiles. *J. Phys. Oceanogr.*, **5**, 369–375.

——, and R. T. Wert, 1976: Temperature–salinity curves in the Pacific and their application to dynamic height computation. *J. Phys. Oceanogr.*, **6**, 613–617.

Flierl, G. R., 1978: Correcting expendable bathythermograph (XBT) data for salinity effects to compute dynamic heights in Gulf Stream rings. *Deep-Sea Res.*, **25**, 129–134.

Ocean Tomography Group, 1982: A demonstration of ocean acoustic tomography. *Nature*, **299**, 121–125.

Olson, D., F. Schott, R. Zantopp and K. Leaman, 1984: The mean circulation east of the Bahamas as determined from a recent measurement program and historical XBT data. *J. Phys. Oceanogr.*, **14** (In press.)

Siedler, G., and L. Stramma, 1983: The applicability of the T–S method to geopotential anomaly computations in the Northeast Atlantic. *Oceanol. Acta*, **6**(2), 167–172.

Stommel, H., 1947: Note on the use of the T–S correlation for dynamic height anomaly computations. *J. Mar. Res.*, **6**, 85–92.

UNESCO, 1981: Tenth report of the joint panel on oceanographic tables and standards. *UNESCO Technical Papers in Marine Science* 36.